Neutron-Diffraction Determination of the Crystal Structure and Magnetic Form Factor of γ-Oxygen*

D. E. Cox, E. J. Samuelsen,† and K. H. Beckurts‡
Brookhaven National Laboratory, Upton, New York 11973
(Received 22 August 1972)

Single-crystal neutron-diffraction data have been used to refine the crystal structure of the paramagnetic cubic γ phase of oxygen at 46 °K. Two of the eight molecules in the $Pm3n$ unit cell are randomly oriented along the ⟨111⟩ axes at the 2(*a*) positions, and the remaining six along the ⟨100⟩ axes perpendicular to the fourfold inversion axes at the 6(*d*) positions. Associated with this disorder is a large librational motion with a rms amplitude of about 20°. Magnetic-form-factor values for 27 reflections have been measured by the polarized-neutron technique. Data were collected from large crystals subjected to an applied magnetic field of about 80 kOe in a specially designed split-coil superconducting magnet. The observed values are in good agreement with theoretical calculations described in the following paper based upon the usual molecular-orbital model with two unpaired electrons in the $p\pi$ antibonding orbitals.

I. INTRODUCTION

Polarized-neutron diffraction has been demonstrated to be a very useful and accurate technique for the determination of magnetic form factors and spin-density distribution in magnetic materials.[1,2] Its application, however, depends upon there being both nuclear and magnetic scattering of appropriate phase contributing to the intensity of the diffracted peaks. This condition is always fulfilled in ferromagnetic materials, but seldom in simple antiferromagnets, and the chief interest to date has therefore, been in the former. A second consideration is the fact that there must be a preponderance of one type of domain, which is not always easy to achieve in antiferromagnets.

It is possible in principle to overcome these difficulties by application of the technique to paramagnetic (or even diamagnetic) materials in an applied magnetic field. In this case, it is the ordered component of the moment in the field direction which produces a polarization effect. In practice, this means that the use of the technique is likely to be limited by factors such as the availability of a high neutron flux, high fields, and large crystals, and relatively few experiments of this type have yet been undertaken.

Oxygen is a particularly interesting magnetic material for this type of study. It is the simplest of the few known materials in which the magnetic properties arise from the presence of unpaired *p* electrons. Moreover, the latter are usually considered in terms of a molecular-orbital model and one must therefore use the appropriate molecular wave functions rather than the customary atomic ones in the interpretation of the results.

The present paper describes a detailed polarized-neutron investigation of the magnetic form factor and spin-density distribution in the paramagnetic cubic γ phase of oxygen in an applied field of 80 kOe. This was made feasible by the development of a split-coil superconducting magnet capable of producing fields of up to 90 kOe, the high neutron flux at the Brookhaven high flux beam reactor, and the fact that large single crystals of γ-oxygen were found to grow quite readily. In addition, a refinement of the crystal structure has been made from unpolarized-neutron data. A quite detailed knowledge of the structure is necessary in any polarized-beam experiment of this sort, and the previous x-ray determination has been considerably extended by the present work, which is described in the first part of the paper. The second part describes the polarized-neutron data collection and analysis. Some of these results have been presented in an earlier short communication.[3] The following paper[4] contains theoretical form-factor calculations based upon molecular wave functions. The observed values are in good agreement with these calculations.

II. CRYSTAL STRUCTURES, MAGNETIC STRUCTURE, AND PHASE TRANSFORMATIONS

Oxygen solidifies at 54.4 °K into the cubic γ phase. At 43.8 °K there is a first-order transformation to the rhombohedral β phase, and at 23.9 °K a further transformation, believed to martensitic, to the monoclinic α phase. The nature of these transformations has been studied by Alikhanov and co-workers,[5,6] Barrett and co-workers,[7–9] and Hörl.[10] At each of the two lower-temperature transitions there is a discontinuous decrease in the magnetic susceptibility by a factor of 2 or so.[11,12] Powder neutron-diffraction measurements have established that α-oxygen is magnetically ordered at 4.2 °K, and that short-range order is present in the β phase at 27 °K.[5,13]

The crystal and magnetic structures of the α

phase have been determined by Alikhanov and coworkers.[6] There are two molecules occupying the corner and body-centered positions of a monoclinic cell with $I2/m$ symmetry (face centered in the equivalent $C2/m$ cell). These are coupled antiferromagnetically with the moments directed along the b axis, and hence perpendicular to the molecular axis. Essentially, the same conclusions were reached in an independent study by Barrett *et al.*,[7] with the exception that the direction of the moments was interpreted as being along the molecular axis, which is, however, inconsistent with the neutron data. Alikhanov *et al.*[14] have also determined form-factor values for the two magnetic reflections observed in $\alpha - O_2$, and find reasonable agreement with theoretical values.

An early attempt to determine the crystal structure of the cubic γ phase was made by Vegard,[15] who reported a cubic close-packed arrangement of rotating O_2-O_2 complexes, with the space group $Pa3$. Substantially the same conclusions were reached shortly afterwards by Keesom and Taconis.[16] A more recent x-ray investigation has been made by Jordan *et al.*[17] and Smith,[18] who assigned the higher-symmetry space group $Pm3n$. The structure shows a high degree of rotational disorder. There are two inequivalent types of oxygen molecules, which are centered at the 2(a) and approximately at the 6(d) positions. Fourier maps indicated a nearly spherical electron density distribution in the 2(a) positions, but an oblate spheroidal distribution about the 6(d) sites (Fig. 1).

Attempts were made to describe the disorder by means of a number of simple models involving various combinations of statistical disorder or free spherical rotation around the 2(a) sites, and statistical disorder or planar rotation around the 6(d) sites. All of these gave a reasonable fit to the x-ray data, but no clearcut choice could be made. Unfortunately, none of the various models was able to account satisfactorily for the intensity data observed in the initial stages of the polarized-beam experiment, and an independent structure determination was therefore carried out with unpolarized neutrons.

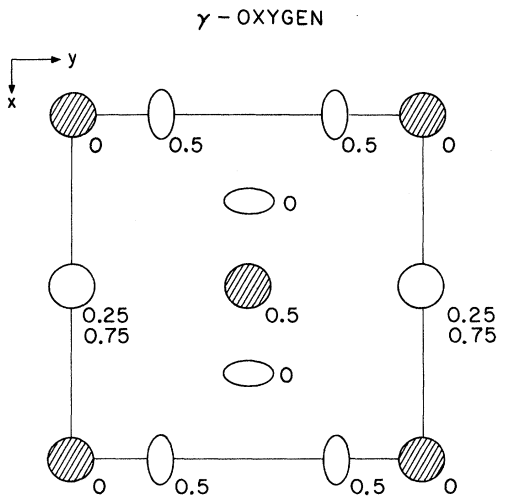

FIG. 1. The crystal structure of γ-O_2 projected on (001) as proposed by Jordan *et al.* (Ref. 17). Molecules at the 2(a) sites at (0, 0, 0) are depicted by shaded circles indicating spherical rotational disorder. Molecules at the 6(d) sites at $(0, \frac{1}{4}, \frac{1}{2})$ show an oblate spherical electron density distribution. Small numerals denote height above the plane.

III. NEUTRON-STRUCTURE REFINEMENT

Single crystals of γ-oxygen were grown in a thin-walled cylindrical aluminum container about 3 mm in diameter and 5 cm long. This was attached to a copper block at the tail section of a variable-temperature helium Dewar. Matheson research-grade oxygen (maximum quoted impurity content less than 10 ppm) was condensed into the container, cooled slowly through the melting point to about 53 °K and held at this temperature overnight. This procedure usually yielded at least one crystal several millimeters in length. Data were collected from two such crystals in the ($hk0$) and (hhl) zones. A deformed germanium monochromator in the (113) position was used to produce the incident neutron beam, of wavelength 1.025 Å. The half-wavelength contamination was found to be negligibly small. The crystal was maintained at 46.0 ± 0.1 °K, and the cell edge at this temperature was determined to be 6.78 ± 0.02 Å.

A total of 25 nonequivalent reflections were measured in the ($hk0$) crystal, and 21 in the (hhl) crystal. Reflections of type (hhl) with l odd were found to be systematically absent, as expected for the space group $Pm3n$ (but not $Pa3$). Measurements were made of at least two and sometimes four equivalent reflections in most cases, and these generally agreed to within 5–10%. Comparable standard errors were assigned to the observed intensities except where the counting statistics gave significantly higher values, which was seldom the case.

In the initial stages of the refinement, a number of models were tried, including those described by Smith.[18] These are summarized in Table I (models A–H). In models A, B, C, and F the bond length of the oxygen molecule is constrained to the value in the gas phase (1.207 Å).[19] In the other models, this constraint is relaxed for at least one of the two types of molecule. Individual isotropic temperature factors were assigned at this stage, and the four strongest peaks were omitted because of appreciable extinction effects. The results of the various refinements are given in Table II. The R factor and

TABLE I. Structural models for γ-O_2 used in least-squares refinement of nuclear-intensity data (see also Refs. 17, 18, and 20).

	Oxygen (I)	Oxygen (II)
A	Spherical around 2(*a*) [molecular center at (0, 0, 0)]	Statistical in 24(*k*) [½ atom at (0, 0.25, 0.4110)]
B	Statistical in 16(*i*) [¼ atom at (0.0514, 0.0514, 0.0514)]	Statistical in 24(*k*) [½ atom at (0, 0.25, 0.4110)]
C	Spherical around 2(*a*) [molecular center at (0, 0, 0)]	Statistical in 24(*k*) [½ atom at (0, *y*, 0.4110)]
D	Spherical around 2(*a*) [molecular center at (0, 0, 0)]	Statistical in 24(*k*) [½ atom at (0, *y*, *z*)]
E	Statistical in 16(*i*) [¼ atom at (*x*, *x*, *x*)]	Statistical in 24(*k*) [½ atom at (0, *y*, *z*)]
F	Spherical around 2(*a*) [molecular center at (0, 0, 0)]	Planar rotor around 6(*d*) [molecular center at (0, ¼, ½)]
G	Spherical around 2(*a*) [molecular center at (0, 0, 0)]	Statistical in 48(*l*) [¼ atom at (*x*, *y*, *z*)]
H	Statistical in 16(*i*) [¼ atom at (*x*, *x*, *x*)]	Statistical in 48(*l*) [¼ atom at (*x*, *y*, *z*)]

weighted R factor are defined as

$$\sum|F_{obs} - F_{calc}| / \sum|F_{obs}|$$

and

$$[\sum w(F_{obs} - F_{calc})^2 / \sum (w F_{obs}^2)]^{1/2},$$

respectively.

Two models give clearly superior agreement, *G* and *H*. The first of these is similar to one which was originally proposed for isostructural β-F_2.[20] The molecules at the 2(*a*) site are assumed to be freely rotating with their bond length fixed at 1.207 Å, while those around the 6(*d*) sites are statistically disordered in the 48(*l*) general positions. The bond length in this case is not constrained to the gas-phase value, but the observed value of 1.18 Å is quite close to this.

Model H differs to the extent that the molecules around the 2(*a*) sites are assumed to be statistically disordered in the 16(*i*) positions at (*x*, *x*, *x*) with a variable parameter, so that the bond length is constrained for neither these nor the 6(*d*) molecules. The values obtained are now 1.04 and 1.17 Å, respectively. The first of these is so low that this model cannot be considered satisfactory in spite of the apparently good intensity agreement.

Anisotropic temperature factors were next introduced into the refinement. Four of the models in Table I gave results far superior to any of the others, and the final parameter values are listed in Table III. All four give excellent agreement, with model H significantly the best with an R factor of only 0.035. The corresponding observed and calculated intensities are given in Table IV. Within experimental error, the molecules around the 6(*d*) sites are statistically disordered within the planes perpendicular to the fourfold axes (Fig. 2) and the observed bond length is 1.24 Å. On the other hand, the 2(*a*) molecules have an apparent bond length of 1.02 Å, which is far less than the gas-phase value. However, the observed amplitudes of vibration along the principal axes of the thermal ellipsoids (Table V) suggest that this foreshortening may be the result of large molecular librations about the [111] axis. If it is assumed that the axial component corresponds to isotropic rigid-body translational motion, then the difference of 0.0535 Å between the mean-square parallel and perpendicular components may be attributed to librational motion about the center of mass. The appropriate correction[21,22] to the bond length is 0.21 Å, giving a corrected value of 1.23 ± 0.03 Å, in good agreement with the gas-phase value. This corresponds to a root-mean-square amplitude of

TABLE II. Results of least-squares refinements for the structural models in Table I with isotropic temperature factors $\exp\{-[(a^2/2\pi^2)U(h^2+k^2+l^2)]\}$. Standard errors are given in parentheses and refer to the least significant digit(s). If no error is given, this particular parameter was kept fixed. R_0 is the molecular bondlength.

	A	B	C	D	E	F	G	H
Oxygen (I)								
x	0.0514	•••	•••	•••	0.0428(32)	•••	•••	0.0442(12)
U(Å^2)	0.117(11)	0.110(13)	0.111(11)	0.104(10)	0.145(19)	0.096(10)	0.103(4)	0.132(8)
R_0(Å)	1.207	1.207	1.207	1.207	1.005	1.207	1.207	1.038
Oxygen (II)								
x	0	0	0	0	0	•••	0.0290(8)	0.0285(12)
y	0.25	0.25	0.244(3)	0.244(2)	0.255(3)	•••	0.2399(9)	0.2413(13)
z	0.411	0.411	0.411	0.415(1)	0.416(1)	•••	0.4179(4)	0.4185(6)
U(Å^2)	0.115(9)	0.111(8)	0.115(8)	0.117(6)	0.112(7)	0.092(6)	0.099(3)	0.095(4)
R_0(Å)	1.207	1.207	1.207	1.153	1.139	1.207	1.181	1.171
R factor	0.259	0.251	0.221	0.171	0.174	0.163	0.061	0.070
Weighted R factor	0.320	0.305	0.284	0.240	0.252	0.234	0.087	0.119

TABLE III. Results of least-squares refinements for some of the structural models in Table I with anisotropic temperature factors. These factors are $\exp[-(a^2/2\pi^2) \times (U_{11}(h^2+k^2+l^2)+U_{12}(2hk+2hl+2kl))]$ for oxygen (I) and $\exp[-(a^2/2\pi^2)(U_{11}h^2+U_{22}k^2+U_{33}l^2+2U_{12}hk+2U_{13}kl+2U_{23}kl)]$ for oxygen (II). Standard errors are given in parentheses, and refer to the least significant digit(s).

	D	E	G	H
Oxygen (I)				
x	...	0.0432(8)	...	0.0436(6)
U_{11} (Å^2)	0.1027(33)	0.1379(46)	0.0966(27)	0.1311(34)
U_{12} (Å^2)	...	−0.0175(23)	...	−0.0180(18)
R_0 (Å)	1.207	1.014	1.207	1.023
Oxygen (II)				
x	0	0	0.0345(7)	0.0340(7)
y	0.2541(18)	0.2542(15)	0.2484(19)	0.2516(20)
z	0.4182(4)	0.4179(4)	0.4156(6)	0.4151(6)
U_{11} (Å^2)	0.1401(30)	0.1391(27)	0.0579(53)	0.0586(51)
U_{22} (Å^2)	0.1075(33)	0.1051(28)	0.1079(24)	0.1063(22)
U_{33} (Å^2)	0.0949(22)	0.0936(19)	0.0949(24)	0.0926(23)
U_{12} (Å^2)	...	...	−0.0090(33)	−0.0038(33)
U_{13} (Å^2)	...	...	−0.0071(19)	−0.0079(18)
U_{23} (Å^2)	−0.0137(43)	−0.0143(37)	−0.0186(33)	−0.0158(34)
R_0 (Å)	1.109	1.114	1.236	1.240
R factor	0.053	0.042	0.043	0.035
Weighted R factor	0.076	0.062	0.055	0.046

libration of about 24°.

Since one might also expect a considerable amount of librational motion to be associated with the 6(d) molecules, it is natural to enquire whether the bondlength of 1.24 Å observed in this case is altogether realistic. With this in mind, model E, although having a rather higher R factor, may offer a physically more satisfactory picture even though the apparent bondlength for the 6(d) molecules is only 1.11 Å. The statistical disorder in this case is restricted to the 24(k) special positions at $(0, y, z)$ (Fig. 2). Reference to Table V shows that the amplitude of vibration along the [100] axis for atoms 1 and 2 is markedly larger than the amplitudes in perpendicular directions. As a rough approximation, the difference of 0.0396 Å^2 between the mean-square parallel component and the average of the mean-square perpendicular components may be attributed to a librational motion about the [100] axis perpendicular to the fourfold inversion axis along [010]. The bondlength corrected in this way is 1.19 ± 0.01 Å. The corresponding value for the 2(a) molecules calculated as before is 1.22 ± 0.04 Å. The root-mean-square angular amplitudes are 19° and 24°, respectively. The observed and calculated intensities for model E are also listed in Table IV.

The final picture is thus one in which the molecules centered at the 2(a) positions orient themselves along one of the ⟨111⟩ axes and the molecules associated with the 6(d) positions lie along one of the ⟨100⟩ axes perpendicular to the fourfold inversion axis at each site. In both cases there is a

TABLE IV. Comparison of observed and calculated structure factors for γ-O_2 at 46 °K for models E and H. Parameters as in Table III. Strong peaks (marked with an asterisk) and unobserved peaks were not included in the refinement. The F_{obs} values have been placed on an absolute basis by dividing out the instrumental scale factor in each case.

	E		H	
	$\lvert F_{calc}\rvert$	F_{obs}	$\lvert F_{calc}\rvert$	F_{obs}
(hk0)				
(110)	0.066	0.066	0.069	0.066
(200)*	2.462	2.100	2.501	2.088
(210)*	2.915	2.423	2.926	2.409
(220)	0.533	0.533	0.526	0.530
(310)	0.229	0.229	0.230	0.228
(320)	0.952	0.976	0.970	0.970
(400)*	1.846	1.802	1.899	1.792
(410)	0.936	0.924	0.913	0.919
(330)	0.488	0.501	0.496	0.498
(420)	0.769	0.779	0.765	0.774
(430)	0.410	0.418	0.424	0.416
(510)	0.167	0.149	0.156	0.149
(520)	0.302	0.280	0.282	0.278
(440)	0.052	0.054	0.055	0.054
(530)	0.186	0.194	0.177	0.193
(600)	0.737	0.819	0.753	0.814
(610)	0.247	0.236	0.242	0.234
(620)	0.349	0.350	0.340	0.348
(540)	0.227	0.222	0.231	0.221
(630)	0.008	<0.05	0.019	<0.05
(710)	0.051	0.054	0.060	0.054
(550)	0.023	<0.02	0.027	<0.02
(640)	0.280	0.279	0.285	0.277
(720)	0.132	0.146	0.154	0.145
(650)	0.143	0.131	0.143	0.130
(800)	0.050	<0.04	0.055	<0.04
(740)	0.010	<0.04	0.045	<0.04
(820)	0.048	0.098	0.077	0.098
(660)	0.018	<0.04	0.022	<0.04
(830)	0.079	0.051	0.050	0.051
(750)	0.059	<0.04	0.042	<0.04
(hhl)				
(110)	0.066	0.073	0.069	0.073
(002)*	2.462	1.952	2.501	1.950
(112)*	2.830	2.246	2.847	2.244
(220)	0.533	0.519	0.526	0.518
(222)	1.330	1.283	1.326	1.282
(004)*	1.846	1.721	1.899	1.719
(114)	0.483	0.480	0.475	0.479
(330)	0.488	0.479	0.496	0.478
(332)	0.279	0.298	0.275	0.298
(224)	0.575	0.580	0.567	0.580
(334)	0.052	0.052	0.049	0.052
(006)	0.737	0.702	0.753	0.701
(442)	0.148	0.142	0.152	0.142
(116)	0.351	0.336	0.339	0.336
(226)	0.062	0.083	0.043	0.083
(444)	0.346	0.368	0.365	0.367
(552)	0.223	0.242	0.228	0.241
(118)	0.137	0.126	0.138	0.126
(554)	0.056	0.065	0.058	0.065
(446)	0.112	0.111	0.105	0.111
(228)	0.075	0.071	0.072	0.070

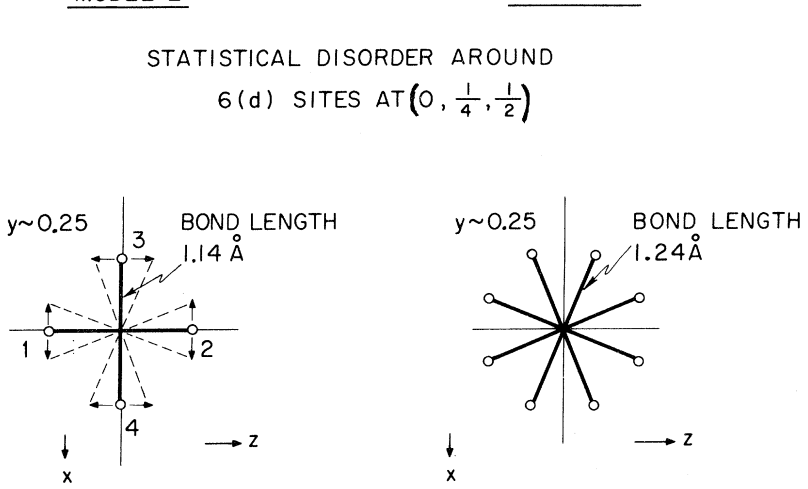

FIG. 2. Statistical disorder around 6(*d*) sites for models E and H. The oxygen atoms are disordered in the 24(*k*) positions at $(0, y, z)$ ($y = 0.2542$, $z = 0.4179$) and the 48(*l*) positions at (x, y, z) ($x = 0.0340$, $y = 0.2516$, $z = 0.4151$), respectively. In model E, there are large molecular librations in the directions indicated by the arrows.

large librational motion having an angular amplitude of roughly 20° superimposed upon a substantial isotropic thermal vibration. This agrees well with the value of 17° deduced by Cahill and Leroi from Raman data.[23] Model H differs from this only to the extent that the molecules are considered to be fixed along directions ± 22° away from the ⟨100⟩ axes rather than undergoing libration about the mean position. It is to be noted that there is a high degree of correlation (− 0.82) between x and U_{11} in the least-squares refinement.

One final point of interest is that application of standard crystallographic significance tests[24] reveals that model E, with statistical disorder in the 2(*a*) sites, has an R factor which is significantly better (at the 0.01 level of confidence) than that of model D, in which there is free spherical rotation about the 2(*a*) sites. The same result is also obtained in a comparison of models H and G. Thus, the presence of free rotation seems rather unlikely.

IV. POLARIZED-BEAM MEASUREMENTS

The split-coil superconducting magnet system was one specially designed to obtain high-field neutron data,[25] and is shown schematically in Fig. 3 (a). The gap between the coils was 0.75 in. The field was monitored by two copper resistance probes which were calibrated at the start of the experiment by means of a third probe placed at the sample position. The field profile along the vertical axis of the magnet is shown in Fig. 3(b), from which the variation over an 0.5-in. vertical sample region is seen to be about 3–4%.

The polarized beam was obtained from a $Co_{0.92}Fe_{0.08}$ crystal and had a wavelength of 1.177 Å. The polarization of the central 0.5-in. region of the beam was about 98%. Polarization was accomplished in the usual way with an rf field of appropriate frequency, which was switched on and off several times a second to minimize the effect

TABLE V. Orientation of the principal axes of the thermal ellipsoids and the corresponding root-mean-square amplitudes of vibration for models E and H.

	Oxygen (I)					
	E			H		
	Amplitude (Å)	Orientation		Amplitude (Å)	Orientation	
$u_{\parallel}$	0.321	[111]		0.309	[111]	
$u_{\perp}$	0.394	⊥[111]		0.386	⊥[111]	
	Oxygen (II)					
	E			H		
	Amplitude (Å)	Angle with cell axes (deg) [100]	[010]	[001]	Amplitude (Å)	Angle with cell axes (deg) [100]	[010]	[001]
u_x	0.373	0	90	90	0.236	18	99	106
u_y	0.339	90	146	56	0.342	89	146	56
u_z	0.290	90	56	34	0.292	72	58	38

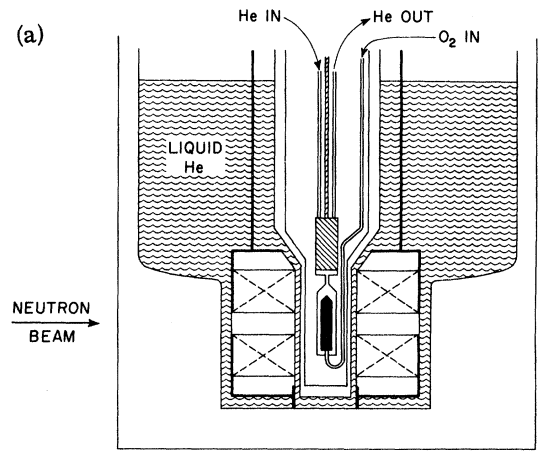

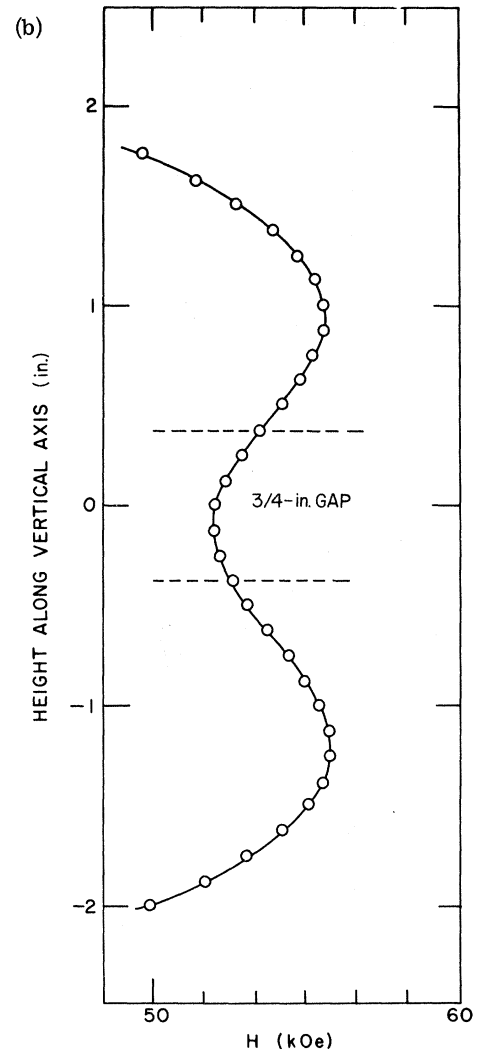

FIG. 3. (a) Schematic diagram of lower portion of superconductor assembly and variable-temperature insert Dewar with oxygen sample holder in place. (b) Typical field profile along vertical axis of superconductor.

of possible long-term fluctuations. The electronics for the two counting channels used for storing data from the two polarization states were interchanged periodically to check for systematic counting errors. The efficiency of polarization reversal was found to be greater than 99%. As pointed out by Steinsvoll *et al.*[26] in a study of Tb, when identical currents circulate in the coils of a symmetric magnet assembly of this kind, there is a small toroidal region where all magnetic field components are effectively zero, and as a result severe depolarization of the neutron beam occurs in this region. However, the latter can be displaced downward by decreasing the current circulating in the lower coil, and a reduction of 15% was found to be effective in eliminating the depolarization effects caused in this way.

Oxygen was condensed into an aluminum sample holder about 1.5 cm in diameter mounted in a variable-temperature Dewar as shown in Fig. 3(a). The temperature of the sample was monitored with a platinum resistor. The resistance of this was measured as a function of applied field at 4.2 and 77 °K, and corrections for magnetoresistance effects at other temperatures were made by means of Kohler's rule.[27]

A number of crystal-growth runs were made as described earlier, and in most cases yielded one large crystal. Data collection was limited to crystals having a zone axis quite close to the vertical as the Dewar was not designed to be tilted more than 5°. Unfortunately, at no time did a large crystal grow with a [100] or [110] axis oriented near to this direction.

A field of 80 kOe was initially applied to the crystals. However, appreciable decay of the current in the two coils took place each day, about 1% and 2% for upper and lower, respectively, and the current was accordingly boosted from time to time to maintain the field between 76 and 80 kOe.

Most of the data were collected from six different crystals, mainly at 46 °K, but at 50 °K in one case. At an early stage it became evident that once the crystal had been allowed to anneal for more than a few hours, a fairly high degree of perfection was attained and the strong peaks were severely affected by extinction. Abnormally low polarization ratios were observed in these cases. Thus, in addition to the peak intensities which are normally measured in polarized-neutron experiments, integrated intensities for both polarization states were measured for several peaks in order to provide a means of correcting for extinction.

A least-squares refinement was performed for each of the sets of data with the magnetic structure factors F_M, an instrumental scale factor K, and an extinction coefficient g as the variable parameters. The other parameters were fixed at the values giv-

TABLE VI. Results of least-squares refinement of polarized-beam data from various crystals of $\gamma-O_2$. The headings IA and IB refer to the same crystal and correspond to data taken after annealing times of a few hours and overnight, respectively. Crystal III could not be aligned properly and no refinement could be made. Polarization ratios indicated that this crystal was free from extinction effects.

	IA	IB	II	III	IV	V	VI
Temperature	46 °K	46 °K	46 °K	46 °K	46 °K	46 °K	50 °K
Orientation	[221]	[221]	[210]	[100]	[210]	[321]	[221]
10^{-3} (Scale factor)	5.9	6.1	0.9	•••	7.5	28.7	23.7
10^{-3} (Extinction parameter)	3.8	5.7	3.2	0.0	4.6	9.6	3.6
R_w	0.177	0.075	0.057	•••	0.080	0.168	0.048

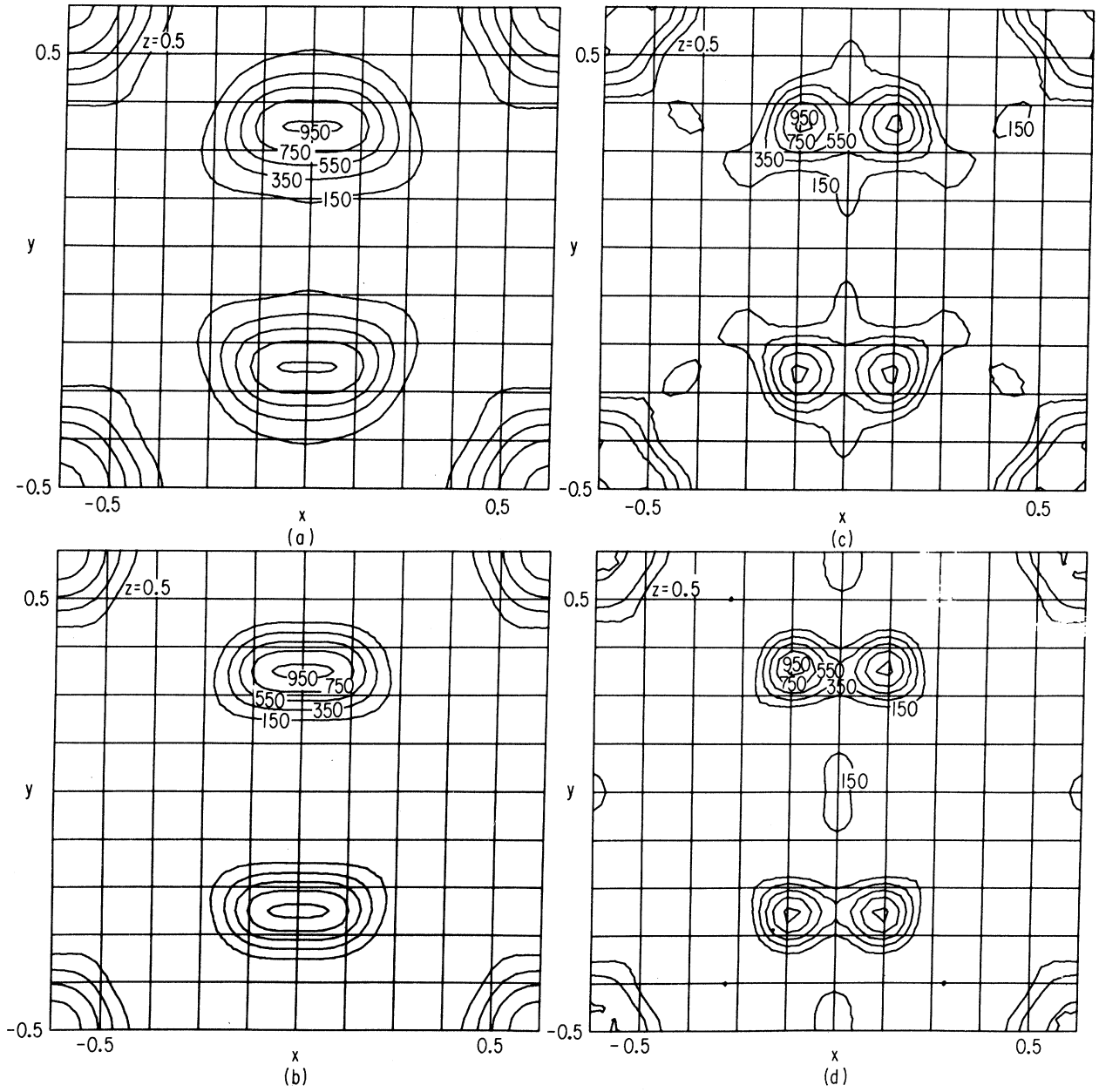

FIG. 4. $z=0.5$ for (a) F_M's at 46 °K, (b) F_N's at 46 °K, (c) F_M's at 0 °K, and (d) F_N's at 0 °K. Small numerals denote contour levels (arbitrary units).

en in Table III for model H. The observed intensity is given by the following expression[28,29]:

$$I^{\pm}_{\rm obs} = KI^{\pm}_{\rm calc}\left|1 + 2\overline{T}g\lambda^3(F_N \pm F_M)^2/V^2\sin2\theta\right|^{-1/2}.$$

$\overline{T}$ is the mean path length (1.25 cm in the present experiment), F_N is the nuclear structure factor, and V is the volume of the unit cell. The other quantities have their usual crystallographic significance. In practice, the term $(F_N \pm F_M)^2$ must be modified slightly to allow for incomplete polarization as described by Nathans *et al.*[30]

The least-squares procedure yields values of K and g which are reasonably well determined, but the refinement is extremely insensitive to variations in the F_M's and these are not well determined at all. However, with the extinction parameter known, corrections can be made to the observed polarization ratios and a reliable set of F_M's can then be determined. The above procedure was repeated in each case with the appropriate set of F_M's fixed at these values. The results for each crystal are listed in Table VI and a typical set of observed corrected and calculated intensities is shown in Table VII. It can be seen that the true net-polarization effect R-1, where $R = I^+/I^-$, may be almost twice its observed value for strong peaks.

Appropriate extinction corrections were also applied to the ratios observed in cases where only the peak heights were measured. The corrections were generally quite small. A check on the reliability of the corrections is given by a comparison of independent measurements on some of the stronger reflections (Table VIII). The over-all consistency is seen to be very good considering the smallness of the polarization effect and the large corrections in several cases.

Values of F_M were derived from the corrected polarization ratios, according to the expression

$$R = I^+/I^- = (1 + 2P\gamma + \gamma^2)/(1 - 2P\gamma + \gamma^2),$$

where $\gamma = F_M/F_N$ and the incident polarization P is 0.98. It has been assumed that the applied field,

TABLE VII. Comparison of observed ($I_{\rm obs}$), extinction-corrected ($I_{\rm corr}$), and calculated ($I_{\rm calc}$) intensities for crystal II. The + and − superscripts refer to values for spin-up and spin-down neutrons, respectively.

(*hkl*)	$I^+_{\rm obs}$	$I^+_{\rm corr}$	$I^+_{\rm calc}$	$I^-_{\rm obs}$	$I^-_{\rm corr}$	$I^-_{\rm calc}$
(200)	881	1670	1798	837	1543	1658
(210)	1102	2249	2077	1060	2112	2056
(211)	1049	2030	1898	1006	1904	1788
(400)	393	522	529	386	510	517
(420)	75	80	78	73	77	77
(421)	63	66	68	64	67	67
(422)	35	36	40	34	35	40
(600)	65	67	61	62	65	60

TABLE VIII. Polarization ratios for some of the more frequently measured reflections from the single crystals of γ-O_2 listed in Table VI. Measured and extinction-corrected values are in left- and right-hand columns, respectively, for each crystal. Standard deviations of counting statistics are given in parentheses and refer to the least significant digit(s). Two listings for a given row and column refer to equivalent reflections.

	IA		IB		II		III		IV		V		VI	
(*hkl*)	$R_{\rm obs}$	$R_{\rm corr}$	$R_{\rm obs}$	$R_{\rm corr}$	$R_{\rm obs}$	$R_{\rm corr}$	$R_{\rm obs}$	$R_{\rm corr}$	$R_{\rm obs}$	$R_{\rm corr}$	$R_{\rm obs}$	$R_{\rm corr}$	$R_{\rm obs}$	$R_{\rm corr}$
(200)	...	...	...	...	1.052(3)	1.080	1.082(5)	1.082	1.050(2)	1.081	...	...	...	...
							1.075	1.075						
(210)	1.038(2)	1.062	1.037(2)	1.066	1.039(5)	1.064	1.070(3)	1.070	1.041(2)	1.072	...	...	1.040(2)	1.066
							1.069(4)	1.069						
(220)	1.054(7)	1.057	1.049(7)	1.052	...	...	...	...	...	...	...	...	1.069(5)	1.071
(420)	1.014(8)	1.015	1.015(8)	1.017	1.016(2)	1.017	...	...	1.018(4)	1.019	1.010(3)	1.013	...	...
(422)	...	...	...	...	1.028(3)	1.029	...	...	1.030(2)	1.031	1.028(4)	1.035	...	...
					1.029(2)	1.030								

TABLE IX. Results of analysis of polarized-neutron data from γ-O_2. Values of F_M have been derived for model H on the assumption that the molecules are at rest and statistically distributed in 16(i) positions (x, x, x) with $x = 0.05139$, and 48(l) positions (x, y, z) with $x = 0.0331$, $y = 0.25$, $z = 0.4174$. For model E the second set of molecules are assumed to be in 24(k) positions ($0, y, z$) with $y = 0.25$, $z = 0.411$. These parameters are chosen to give the gas-phase bond length of 1.207 Å. Standard deviations of counting statistics are given in parentheses and refer to the least significant digit(s).

			H (0 °K)		E (0 °K)	
(hkl)	γ	$\sin\theta/\lambda$	F_N (10^{-12} cm)	F_M (10^{-12} cm)	F_N (10^{-12} cm)	F_M (10^{-12} cm)
(110)	0.0109(20)	0.104	0.115	−0.0125(23)	0.119	0.0130(24)
(200)	0.0200(10)	0.147	2.819	0.0564(28)	2.852	0.0570(29)
(210)	0.0169(10)	0.165	3.621	0.0612(36)	3.615	0.0611(36)
(211)	0.0169(24)	0.181	3.619	0.0612(87)	3.614	0.0611(87)
(220)	0.0149(24)	0.209	−0.739	−0.0110(18)	−0.835	−0.0124(20)
(310)	0.0215(35)	0.233	0.411	0.0088(14)	0.384	0.0083(14)
(222)	0.0098(7)	0.255	−2.042	−0.0200(14)	−1.851	−0.0181(13)
(320)	0.0078(13)	0.266	−1.443	−0.0113(19)	−1.412	−0.0110(18)
(321)	0.0074(15)	0.276	1.819	0.0135(27)	1.845	0.0137(28)
(400)	0.0058(10)	0.295	3.382	0.0196(20)	3.826	0.0222(38)
(410)	0.0138(30)	0.304	−2.003	−0.0276(60)	−1.867	−0.0258(56)
(411)	0.0110(19)	0.313	−1.389	−0.0153(26)	−1.384	−0.0152(26)
(330)	0.0121(20)	0.313	0.715	0.0087(14)	0.986	0.0119(20)
(420)	0.0042(7)	0.330	1.815	0.0076(13)	1.517	0.0064(11)
(421)	0.0024(9)	0.338	1.619	0.0039(15)	1.748	0.0042(16)
(422)	0.0080(13)	0.361	1.710	0.0137(22)	1.832	0.0147(24)
(430)	0.0044(34)	0.369	−1.395	−0.0061(47)	−1.867	−0.0082(63)
(431)	0.0098(21)	0.376	−0.487	−0.0048(10)	−0.514	−0.0050(11)
(432)	−0.0110(50)	0.397	−0.048	0.0005(2)	0.455	−0.0050(23)
(521)	−0.0019(25)	0.404	−0.534	0.0010(13)	−0.184	0.0003(4)
(531)	0.0051(40)	0.436	0.0	0.0(0)	0.0	0.0(0)
(600)	0.0063(9)	0.442	−4.710	−0.0297(33)	−3.083	−0.0194(22)
(442)	−0.0048(21)	0.442	0.660	−0.0032(14)	1.149	−0.0055(24)
(532)	0.0158(16)	0.455	−0.838	−0.0132(13)	−1.254	−0.0198(20)
(621)	0.0046(15)	0.472	−2.301	−0.0106(35)	−1.632	−0.0075(24)
(542)	0.0101(31)	0.495	−1.552	−0.0157(48)	−2.380	−0.0240(74)
(444)	0.0075(8)	0.511	−2.208	−0.0166(18)	−4.230	−0.0317(34)

and hence the polarization axis, are perpendicular to the scattering vector. While this is not strictly valid if the Dewar is tilted, the corrections were found to be negligibly small for tilts of 5° or less. γ was determined for 27 reflections in all, including all those out to (421), in many cases the values being average ones derived from several independent measurements. All values have been normalized to an applied field of 80 kOe on the basis of a linear field dependence, which should be a good approximation at this temperature.

The 46 °K data can be used in conjunction with the known values of F_N to give a set of F_M's directly, both in magnitude and sign. From these, a three-dimensional Fourier synthesis can be made, and sections at $z = 0.5$ are shown for magnetic and nuclear scattering in Figs. 4(a) and 4(b), respectively. The value of $F_M(000)$ was calculated from the susceptibility measurements of Kanda *et al.*[10] on the assumption that these can be linearly extrapolated to 80 kOe.

The effect of the large thermal librational motion tends to smear out details of the maps, and one would like to find a way of eliminating these effects if possible. It is not possible to obtain data at lower temperatures of course because of the structural transition at 44 °K. However, the basically simple picture of the librational motion described in Sec. III sugests a simple model for the temperature dependence of the cubic structure were it stable from 0 °K to the melting point. The effect of lowering the temperature would be to decrease the amplitude of the molecular librations until at 0 °K the structure would be just a statistical distribution of the two types of molecules about their respective centers as before, but with no librational motion superimposed. This is admittedly rather arbitrary and neglects zero-point motion, but it does give a physically reasonable means of extrapolating the data to lower temperatures. In this way, a set of effective F_N's at 0 °K can be calculated, on the assumption that the intranuclear separation is the same as in the gas phase, 1.207 Å. One would not expect this to change much in the solid, and the corrected bondlengths found in the present study, and also those found by Barrett

et al.[7] in an x-ray study of the monoclinic phase at 23 °K, support this assumption. The F_N values calculated on this basis and the derived F_M values are listed in Table IX, and corresponding Fourier sections are shown in Figs. 4(c) and 4(d). Series termination effects are undoubtedly substantial, but the qualitative features of the spin density distribution are nevertheless quite evident.

Good agreement between observed and calculated F_M's is obtained with the simple model proposed by Leoni and Sacchetti.[4] In this, the molecular disorder in the two sets of positions is approximated by probability functions with spherical and ellipsoidal distributions respectively.

The form factor can be expressed in terms of a spherical and an aspherical contribution, and temperature dependence can be allowed for in a simple fashion by variation in the ellipsoidal distribution function without explicit consideration of the thermal factors or librational motion. A detailed description of these calculations is given in the following paper.[4]

ACKNOWLEDGMENTS

Experimental assistance from F. Langdon is gratefully acknowledged, as also are helpful discussions with F. Leoni, M. Blume, and R. Nathans. We are indebted to Dr. H. W. Smith for supplying a copy of his thesis and to Dr. R. A. Alikhanov for supplying a translated preprint of his paper prior to publication. Two of the authors (E. J. S. and K. H. B.) would like to express gratitude for the hospitality experienced during their stay at Brookhaven National Laboratory.

---

*Work performed under the auspices of the U. S. Atomic Energy Commission.

†Guest, now returned, from Institutt for Atomenergi, Kjeller, Norway.

‡Guest, now returned, from Kernforschungsanlage Jülich GMBH, Jülich, West Germany.

[1]R. Nathans, C. G. Shull, G. Shirane, and A. Andresen, J. Phys. Chem. Solids 10, 138 (1959).

[2]R. Nathans and S. J. Pickart, *Magnetism* (Academic, New York, 1963), Vol. III, p. 211.

[3]D. E. Cox, E. J. Samuelsen, and K. H. Beckurts, J. Phys. 32, C582 (1971).

[4]F. Leoni and F. Sacchetti, following paper, Phys. Rev. 7, 3112 (1973).

[5]R. A. Alikhanov, Zh. Eksp. Teor. Fiz. 45, 812 (1963) [Sov. Phys.-JETP 18, 556 (1964)]; J. Phys. 25, 449 (1964).

[6]R. A. Alikhanov, E. B. Vul, and J. G. Fedorov, Acta Cryst. 21, Suppl. A92 (1966); R. A. Alikhanov, Zh. Eksp. Teor. Fiz. Pis'ma Red. 5, 430 (1967) [JETP Lett. 5, 349 (1967)].

[7]C. S. Barrett, L. Meyer, and J. Wasserman, J. Chem. Phys. 47, 592 (1967).

[8]C. S. Barrett and L. Meyer, Phys. Rev. 160, 694 (1967).

[9]C. S. Barrett, L. Meyer, and J. Wasserman, Phys. Rev. 163, 851 (1967).

[10]E. Hörl, Acta Cryst. B25, 2515 (1969).

[11]A. S. Borovic-Romanov, M. P. Orlova, and P. G. Strelkov, Dokl. Akad. Nauk. SSSR 99, 699 (1954).

[12]E. Kanda, T. Haseda, and A. Otsubo, Physica 20, 131 (1954); Sci. Rept. Res. Inst. Tohoku Univ. 7, 1 (1955).

[13]M. F. Collins, Proc. Phys. Soc. (London) 89, 415 (1966).

[14]R. A. Alikhanov, I. L. Ilyina, and L. S. Smirnov Phys. Status Solidi B 50, 385 (1972).

[15]L. Vegard, Z. Phys. 98, 1 (1935).

[16]W. H. Keesom and K. W. Taconis, Physica 3, 141 (1936).

[17]T. H. Jordan, W. E. Streib, H. W. Smith, and W. N. Lipscomb, Acta Cryst. 17, 177 (1964).

[18]H. W. Smith, Ph. D. thesis (Harvard University, 1966) (unpublished).

[19]G. Herzberg, *Molecular Spectra and Molecular Structure*, 2nd ed. (Van Nostrand, New York, 1950), p. 560.

[20]T. N. Jordan, W. E. Streib, and W. N. Lipscomb, J. Chem. Phys. 41, 760 (1964).

[21]W. R. Busing and H. A. Levy, Acta Cryst. 17, 142 (1964).

[22]W. C. Hamilton and J. A. Ibers, *Hydrogen Bonding in Solids* (Benjamin, New York, 1968), p. 60.

[23]J. E. Cahill and G. E. Leroi, J. Chem. Phys. 51, 97 (1969).

[24]W. C. Hamilton, Acta Cryst. 18, 502 (1965).

[25]F. T. Langdon (unpublished).

[26]O. Steinsvoll, G. Shirane, R. Nathans, and M. Blume, Phys. Rev. 161, 499 (1967).

[27]M. Kohler, Ann. Phys. 32, 106 (1938).

[28]W. H. Zachariasen, Acta Cryst. 23, 558 (1967).

[29]P. Coppens and W. C. Hamilton, Acta Cryst. A26, 71 (1970).

[30]R. Nathans, H. A. Alperin, S. J. Pickart, and P. J. Brown, J. Appl. Phys. 34, 1182 (1963).